 doi:10.20944/preprints202008.0573.v1

Microstructure and the local mechanical properties of the 3D printed austenitic stainless steel: Computer simulation

Hamed Hosseinzadeh[1, *]

[1] Henry M. Rowan College of Engineering, Rowan University, NJ

* Corresponding author:

Email address: Hamed@uwalumni.com

Address: Rowan University, 201 Mullica Hill Road, Glassboro, New Jersey 08028

Abstract

Metal 3D printing technology is a promising manufacturing method, especially in the case of complex shapes. The quality of the printed product is still a challenging issue for mechanical applications. The anisotropy of the microstructure, imperfections, and residual stress are some of the issues that diminish the mechanical properties of the printed sample. The simulation could be used to investigate some technical details, and this research has tried to computationally study the metal 3D printing of austenitic stainless steel to address austenite microstructure and local yield strength. Two computational codes were developed in Visual basics 2015 to simulate the local heating/cooling curve and subsequent austenite microstructure. A stochastic computational code was developed to simulate austenite grain morphology based on calculated thermal history. Then Hall-Pitch equation was used to estimate the yield strength of the printed sample. These codes were used to simulate the effect of temperature of the printer's chamber on microstructure and subsequent yield strength. The austenite grain topology is more columnar at a lower temperature. The percentage of the equiaxed zone will be increased at a higher chamber's temperature. Almost a fully equiaxed austenite microstructure will be achieved at 800 C chamber's temperature, but the last printed layer, which is columnar and can be removed by cutting then. The estimated local austenite grain size and the local yield strength in the equiaxed regions are in the range of 15 to 30 µm and 270 to 330 MPa at 800 C temperature of printer's chamber, respectively.

Keywords: 3D printing, stainless steel, microstructure, mechanical properties, simulation

 doi:10.20944/preprints202008.0573.v1

- **Introduction**

ASTM Standard F2792 has categorized additive manufacturing processes as Directed Energy Deposition (DED) and Powder Bed Fusion (PBF). Generally, the additive manufacturing process is using a heat source to deposit the melted materials layer by layer. 3D printing is a kind of rapid prototyping, and metal 3D printing can be beneficial for producing non-structural applications for design purposes [1]. Recently, metal 3D printing became more popular, and the microstructure/mechanical properties of the printed sample were experimentally studied [2–7]. Mechanical properties and microstructure of the metal 3d printed samples are not fully reliable for applications, especially for load-bearing parts. So, printed samples need additional postprocessing [8, 9], and the effect of heat treatment on mechanical properties/microstructure needs to be studied in detail [10]. Thermal history during printing and melting/solidification conditions are controlling subsequent microstructure, then mechanical properties [11]. The simulation gives many details about thermal history during printing [7, 12–15]. There is some research that coupled macroscale thermal simulation coupled with mesoscale microstructural evaluation [16–19]. There are several published kinds of research on mesoscale microstructural simulations for powder bed-based additive manufacturing in the first layer of the print [20–25]. In addition, there are researches on addressing the grain structure of the additively manufactured materials, especially for powder bed fusion [25–28]. Computational phase transformation or phase fraction based on the continuous cooling curves and phase diagrams are still limited for metal 3D printing. Still, there are published researches on welding, which is very close to metal additive manufacturing [29]. Computational prediction of phase transformation in steel is more challenging than grain morphology prediction, which could be simply studied computationally [30, 31]. Phase transformation simulation could be done and simplified by the use of phase diagrams and a continuous cooling curve to predict the phase percentages [32].

This research is a process modeling of metal 3D printing of austenite stainless steel with a direct laser deposition (DLD) method. The effect of temperature of the printer's chamber on microstructure and yield strength of the printed sample was studied.

- **Computational method**

In this research, a multiscale multiphysics computational code was developed in Visual Basic 2015. The computational outputs of this code are 3D thermal and microstructural (grain size) history during metal 3D printing of austenite stainless steel. It has two major computational algorithms i. *Thermal analysis* and ii. *The microstructural analysis* which are discussed in the following topics. The yield strength is calculated by the Hall-Petch equation and calculated austenite grain size. Fig 1 shows the computational algorithm of the multiscale and multiphysics simulation of this research.

Preprints (www.preprints.org) | NOT PEER-REVIEWED | Posted: 26 August 2020 doi:10.20944/preprints202008.0573.v1

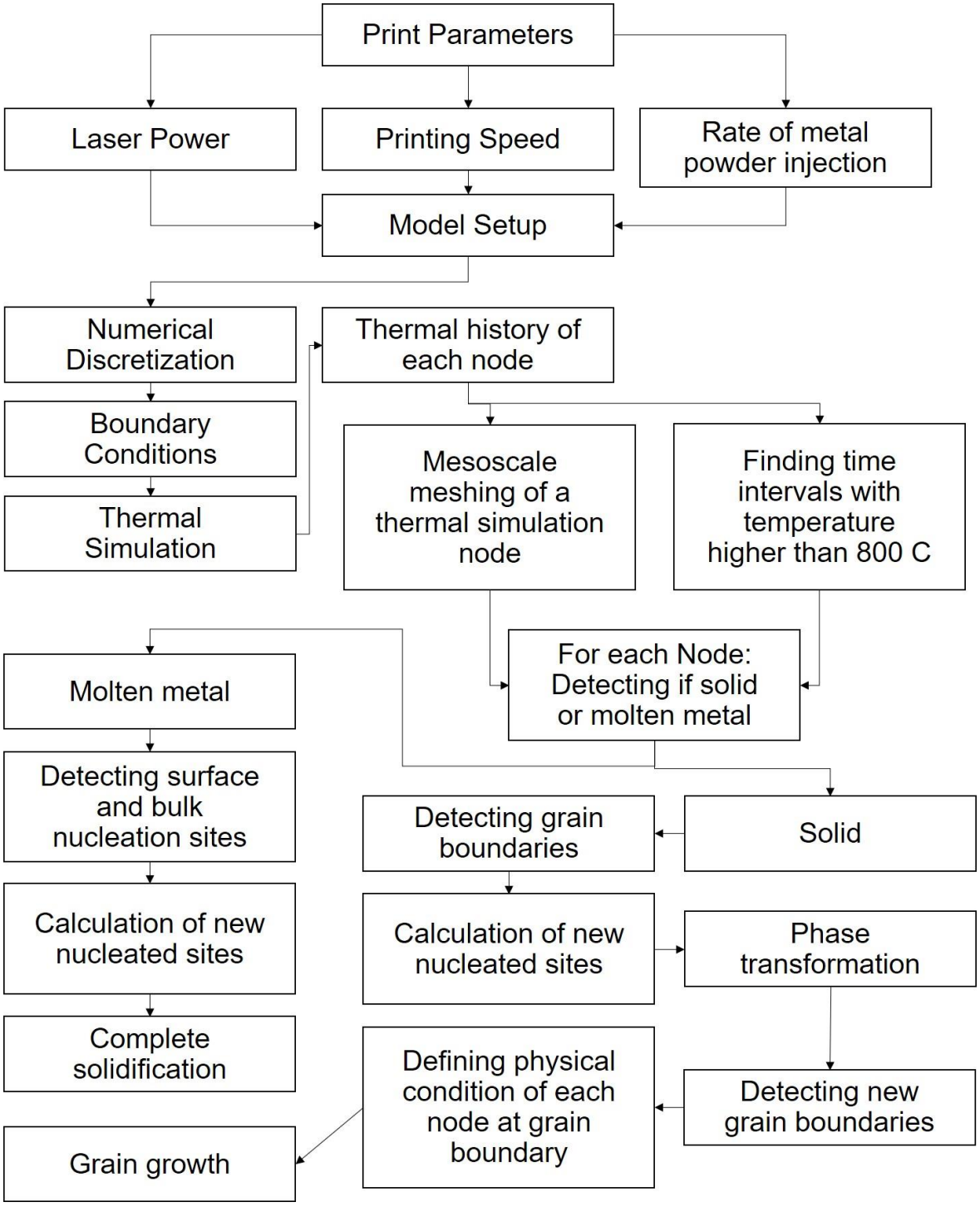

Fig. 1 – The computational algorithm of the multiscale and multiphysics simulation of this research. The developed computational algorithm for the prediction of austenite grain size according to thermal history.

Preprints (www.preprints.org) | NOT PEER-REVIEWED | Posted: 26 August 2020 doi:10.20944/preprints202008.0573.v1

- Thermal analysis

Equation 1 was used for thermal analysis in which ρ is density, C_p is the specific heat, T is temperature, t is time, λ is the thermal conductivity, and Q is the source of heat.

$$\rho C_p \frac{\partial T}{\partial t} = \nabla.(\lambda \nabla T) + Q \qquad (1)$$

Equation 1 was solved by the finite difference method. In metal 3D printing, we have metal powders that are blown to the laser to be melted by laser and thus, adding a new layer during metal 3D printing. To tackle this subject, new nodes (for newly melted powders which are added from the nozzle) will be added to the defined position (exactly under the nozzle) on the previously printed part of the model during each time step. This is the used method to update the model to consider newly melted metal powders through the nozzle.

For the laser heat source, power distribution is in the range of a millimeter [1]. In this research, we considered a constant temperature for melted powders as the initial condition rather than using laser energy and conventional Gaussian surface heat source, top-hat distribution, or Goldak's double ellipsoid heat source [33] as a boundary condition. The higher temperature of melted powders means higher laser power.

The rest of the simulation domain, which is not under the effect of the printer nozzle (direct contact with the laser), exchanges the heat between the surface of the printed sample and the environment. The energy balance (equation 2) was applied as a thermal boundary condition. This equation has the physical meaning of both thermal convection and radiation. h represents both the thermal convection and radiation coefficients. The value of β was considered to be 0.9, as recommended for hot-rolled steels [34].

$$-\nabla.(\lambda_i \nabla T) = h(T - T_\infty) \qquad (2)$$

$$h = 0.00241 \times \beta \times T^{1.61}$$

- Microstructural analysis

Austenite grain growth is one of the important subjects that will control the final mechanical and physical properties of the fabricated metallic sample. The grain growth of austenite was quantitatively simulated according to the calculated local thermal history of the printed model. Stochastic computational algorithms were developed to simulate i. *Austenite nucleation*, ii. *Austenite formation*, and iii. *Austenite grain growth*. The stochastic method uses kinetic equations of phase nucleation and formation to define the chance of phase transformation of each point in the discretized model. These kinetic equations need thermal history and heating/cooling curve between 800 C to the melting point. The thermal range of 800 C to the melting point was considered high enough to change the microstructure. Surface energy or surface tension (surface curvature) of each austenite grains is also controlling microstructure shape and needs to be considered in the simulation. A weighted coordination number was used for each point (a node in the discretized model) to account for the surface energy of each austenite grain. In the discretized model, each point has three kinds of neighbors. The neighbor has shared surface contact, the one which shares a contact by line, and the last one has point contact, and

Preprints (www.preprints.org) | NOT PEER-REVIEWED | Posted: 26 August 2020 doi:10.20944/preprints202008.0573.v1

they are were weighted by 1, 0.75, and 0.25, respectively. During the simulation, computational code is checking all the neighbors of each point and detects the neighbors. Based on this and the defined weighted number for each neighbor, a new number is assigned to each computational point, which is the summation of all the weighted numbers of the same neighbors. If this number is 19, it means that this point is inside its grain (austenite grain in this simulation). If it is lower than 19, it means that this point is at the grain boundary. Besides the effect of temperature on grain growth, this number is also controlling the microstructural evolution and its shape. The higher weighted number means more neighbors and a more stable position (lower surface energy) than the case with a lower weighted number. So, the chance of leaving a point from the current position to be part of the neighbor austenite grain is higher if the number is lower.

Probability number for austenite grain growth ($P_{grain\ growth}$) was defined based on its grain boundary velocity ($V_{grain\ growth}$) and the weighted coordination number. The used equation is:

$$P_{grain\ growth} = \frac{V_{grain\ growth}.dt}{dx} \times (Weighted\ number) \qquad (3)$$

$$V_{grain\ growth} = 1.67 \times 10^{-7} e^{(\frac{-124500}{8.314T})} \qquad (4)$$

T is temperature, dt is a simulation time scale, and dx is the numerical mesh size. More details about the used stochastic method for microstructural simulation were explained in reference [34] by the author.

- **Results and discussions**

Local temperature variation of the printed layers directly controls the microstructure, and the local microstructure will affect the final mechanical properties. In this research, the temperature distribution was simulated, and the heating/cooling curves for some points of the printed sample have been extracted. Fig. 2 shows the defined points which were used to extract the temperature variations during printing. The simulated results are shown in fig. 3 for point P11, P12, P21, P22, P31, and P32 due to the symmetry. The laser power (or equivalent temperature), print speed, and powder's feeding rate were kept constant in this simulation. The laser power assumed to be enough to reach the melting powders to 1800 C. The print speed and powder's feeding rate were 2 mm per second and 100 mg per second, respectively. The local temperature's variations have been simulated at different chamber's temperatures. Four temperatures of the printer's chamber have been checked (25, 700, 750, and 800 C).

Preprints (www.preprints.org) | NOT PEER-REVIEWED | Posted: 26 August 2020 doi:10.20944/preprints202008.0573.v1

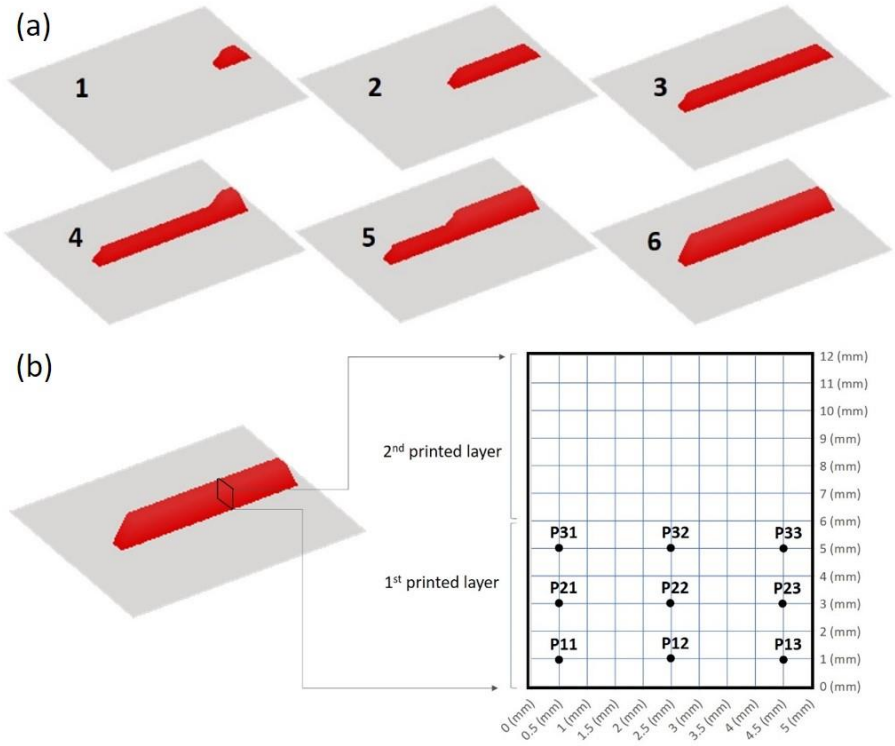

Fig. 2 – (A) Schematic shows how recently melted metal powders will be added to the model during each time step of simulation to construct layers on each other, and (b) shows the size of a cross-section with some points.

Preprints (www.preprints.org) | NOT PEER-REVIEWED | Posted: 26 August 2020 doi:10.20944/preprints202008.0573.v1

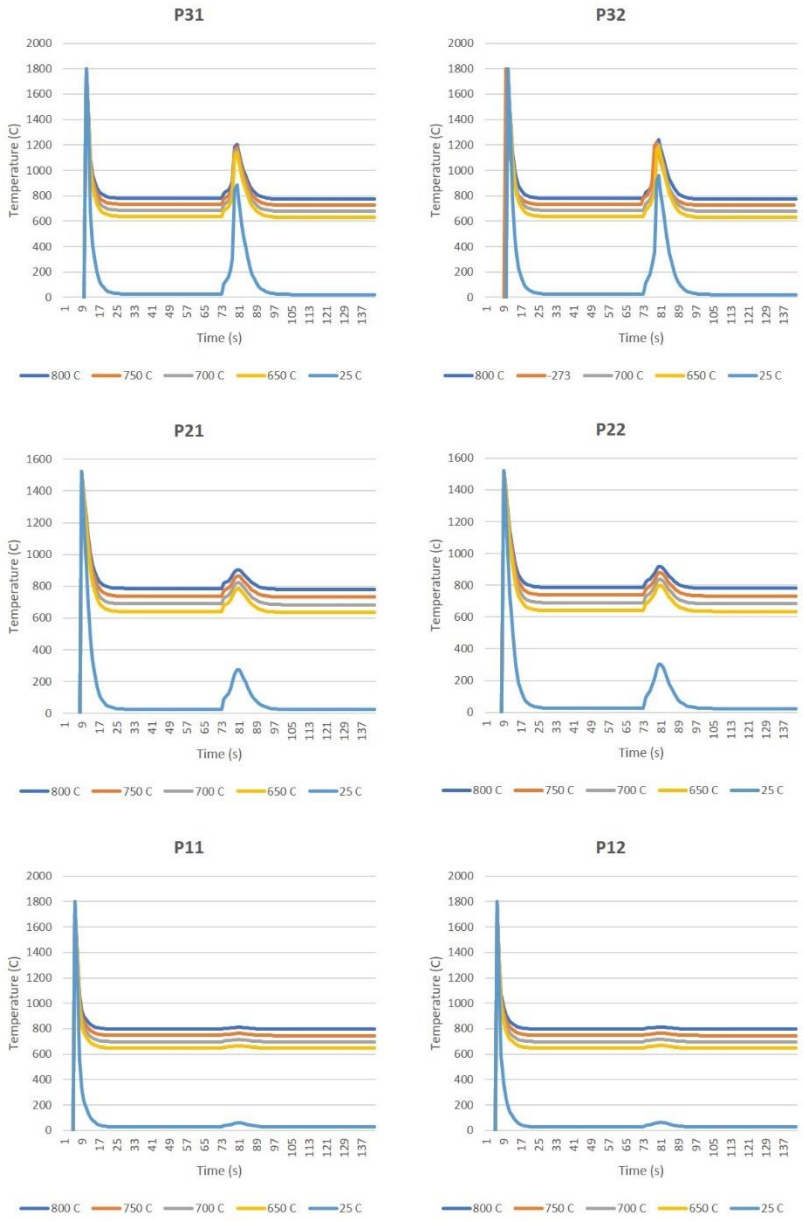

Fig. 3 – Simulated temperature profiles at different positions and temperatures of the printer's chamber.

If any points reheated again due to the heat of the last printed layer, but it could not reach the temperature higher than 800 C (the approximate limit temperature that could affect the microstructure), it means the microstructure will not be affected by temperature significantly. So, there is no substantial microstructural evolution, and the solidified microstructure will also remain unchanged at least austenite grain morphology. But if any point reheats and experiences temperatures higher than 800 C, the microstructure will be changed from a solidified microstructure. The solidified microstructure has mainly columnar grain structure, which has been grown in the direction of the head flow during cooling. So, the mechanical properties of the solidified microstructure are anisotropic. The regions

Preprints (www.preprints.org) | NOT PEER-REVIEWED | Posted: 26 August 2020 doi:10.20944/preprints202008.0573.v1

reheated by the temperature higher than 800 C would have an equiaxed microstructure, and the mechanical properties would be isotropic.

Microstructural evolution, which is a direct consequence of local heating and cooling conditions, was simulated and studied by a stochastic model. This is a mesoscale simulation and a cube with a size of $210\ \mu m \times 210\ \mu m \times 210\ \mu m$ was extracted from different positions of the printed model to compare. The calculated thermal history was used as an input for microstructural evolution in the stochastic model. This cube was discretized by 343000 numbers of computational elements, which means 3 µm mesh size. The overall concept of the stochastic model is based on the physical-based probability number, which is assigned to each computational element. For example, if the whole cube is liquid and it is at the solidification temperature or lower, a probability number based on the kinetics of solidification will be assigned to each computational element of the discretized cube and if a produced random number by computer is higher than the probability number, the state of that element will be changed to the solid from the liquid. There is the same scenario for new austenite nucleation, phase transformation of ferrite/pearlite to austenite, and austenite grain growth.

If the temperature of the extracted cube from the printed model is higher than 1500 C, it is a melted zone (liquid metal). Solidification will start with homogenous and heterogeneous nucleation at 1500 C and lower. We used the function (probability number) in equation 5 to decide the state of each element if it is liquid or solid:

$$P_{Solidification} = e^{-Q/(KT)} \qquad (5)$$

Where $K$is Boltzmann's constant, T is temperature, and Q is the activation energy. The values for Q are considered $1 \times 10^{-19}\ J$ and $1.8 \times 10^{-17}\ J$ for heterogenous and homogenous nucleations, respectively. Although the exact grain sizes after solidification and grain growth are sensitive to Q number, the physical prediction of the microstructure is reliable by the used Q number in this research, and computational estimation of the position of fine or coarse austenite grains in the model is not affected by Q value too much.

The as solidified microstructure has a columnar grain structure in the direction of heat flow during cooling and solidification. The new austenite grains will start to nucleate and grow if the sample reheated again at a temperature higher than 800 C. Printed samples in the chamber with a temperature higher than 700 C experienced local temperature in some points higher than 800 C when reheated again. Hence, we have austenite grains nucleation and growth in some parts of the samples. This subject shows in fig. 4, fig. 5, and fig. 6. If a uniform microstructure is a goal, only the chamber's temperature at or higher than 800 C could eliminate the columnar regions but the last printed layer (top printed layer), which can be removed then.

Preprints (www.preprints.org) | NOT PEER-REVIEWED | Posted: 26 August 2020 doi:10.20944/preprints202008.0573.v1

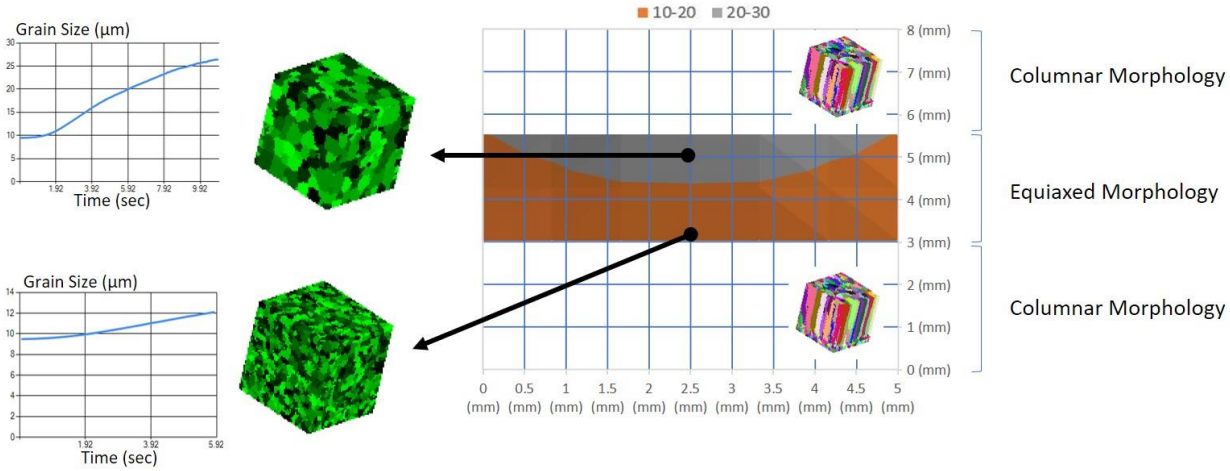

Fig. 4 – Simulated austenite grain size, grain morphology, and its map at 700 C temperature of the printer's chamber.

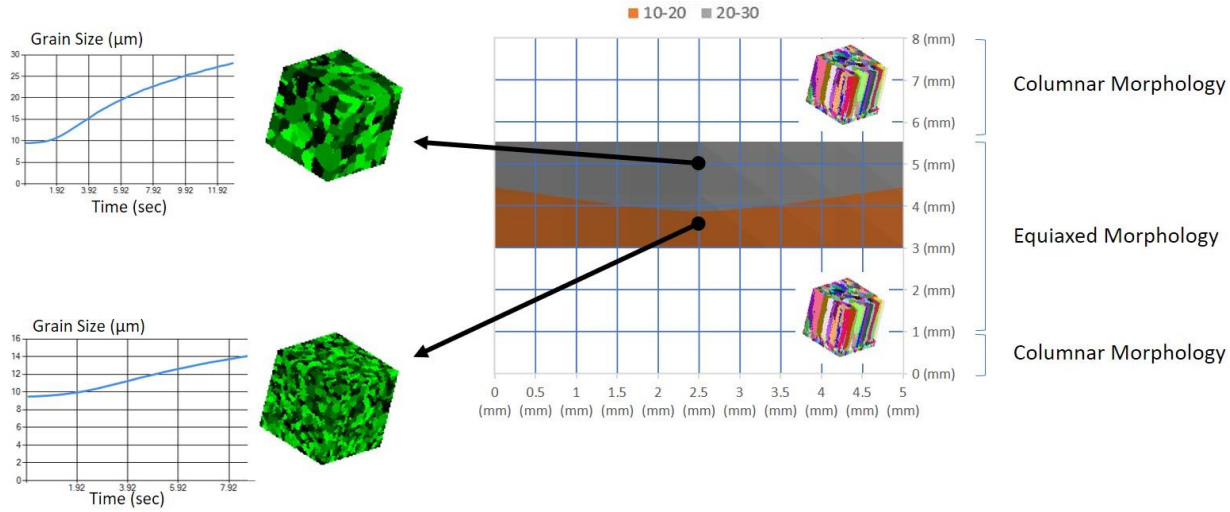

Fig. 5 – Simulated austenite grain size, grain morphology, and its map at 750 C temperature of the printer's chamber.

Preprints (www.preprints.org) | NOT PEER-REVIEWED | Posted: 26 August 2020 doi:10.20944/preprints202008.0573.v1

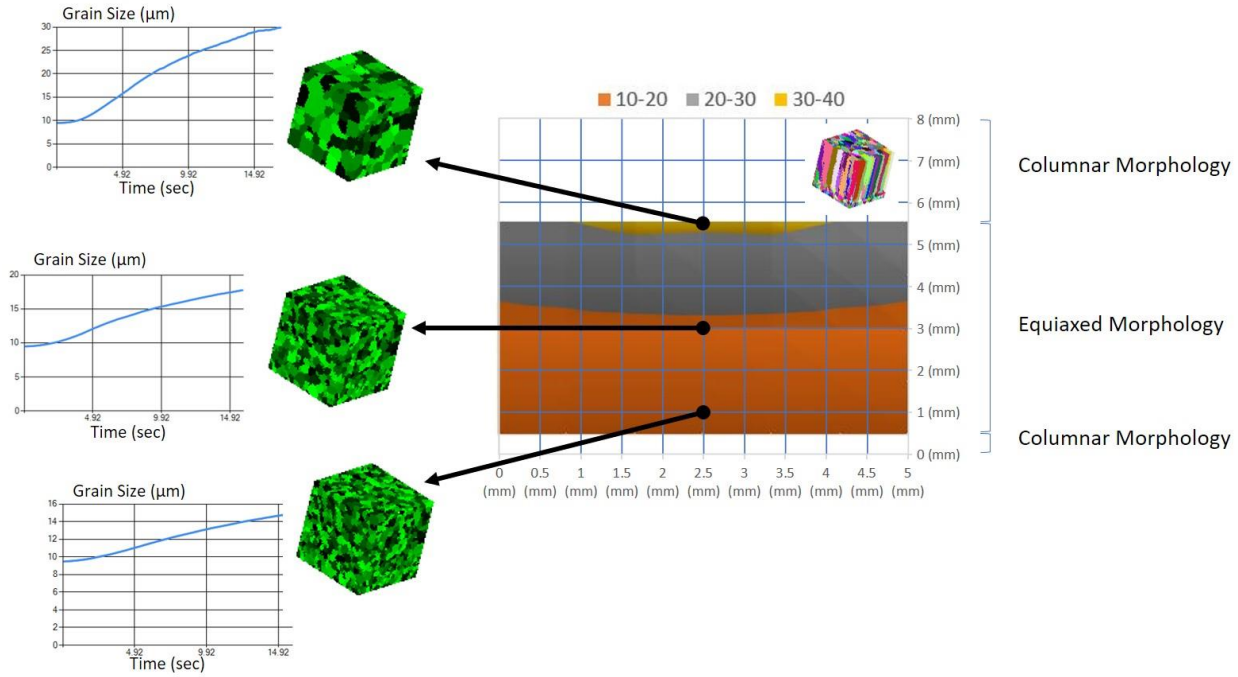

Fig. 6 – Simulated austenite grain size, grain morphology, and its map at 800 C temperature of the printer's chamber.

If the microstructure is equiaxed austenite grain, the yield strength could be calculated by the Hall-Pitch equation. Fig. 7, fig. 8, and fig. 9 show the map of yield strength in the equiaxed region of the printed sample at different temperatures of the printer's chamber.

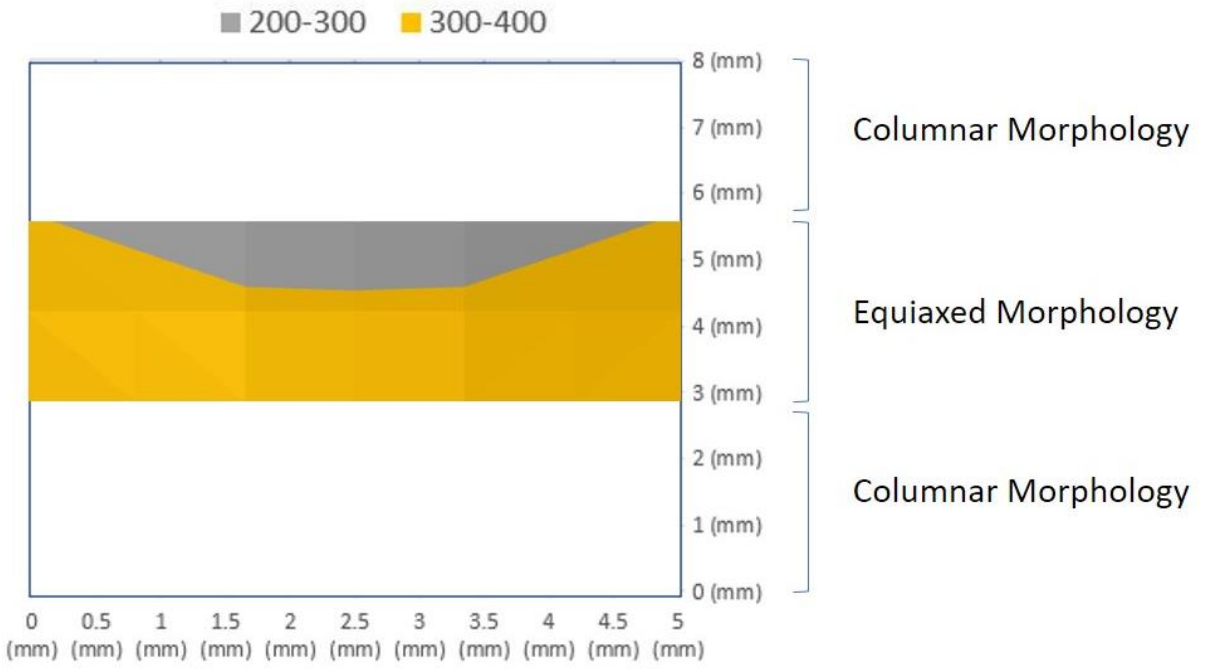

Fig. 7 – Calculated yield strength and its map at 700 C temperature of the printer's chamber.

Preprints (www.preprints.org) | NOT PEER-REVIEWED | Posted: 26 August 2020 doi:10.20944/preprints202008.0573.v1

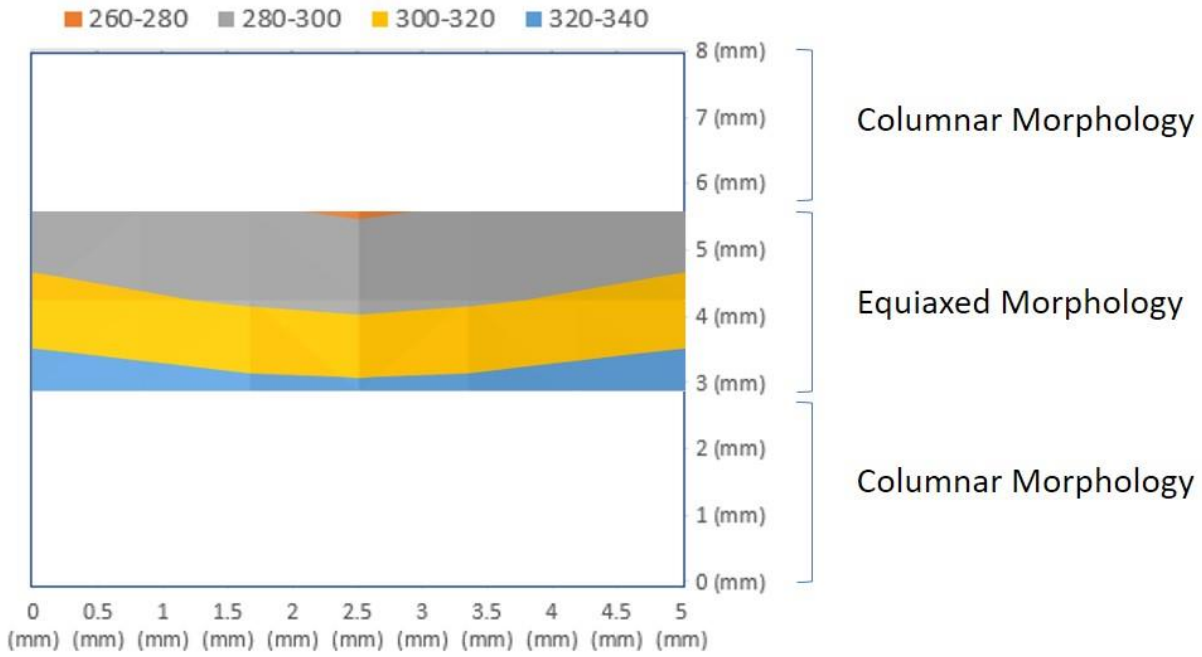

Fig. 8 – Calculated yield strength and its map at 700 C temperature of the printer's chamber.

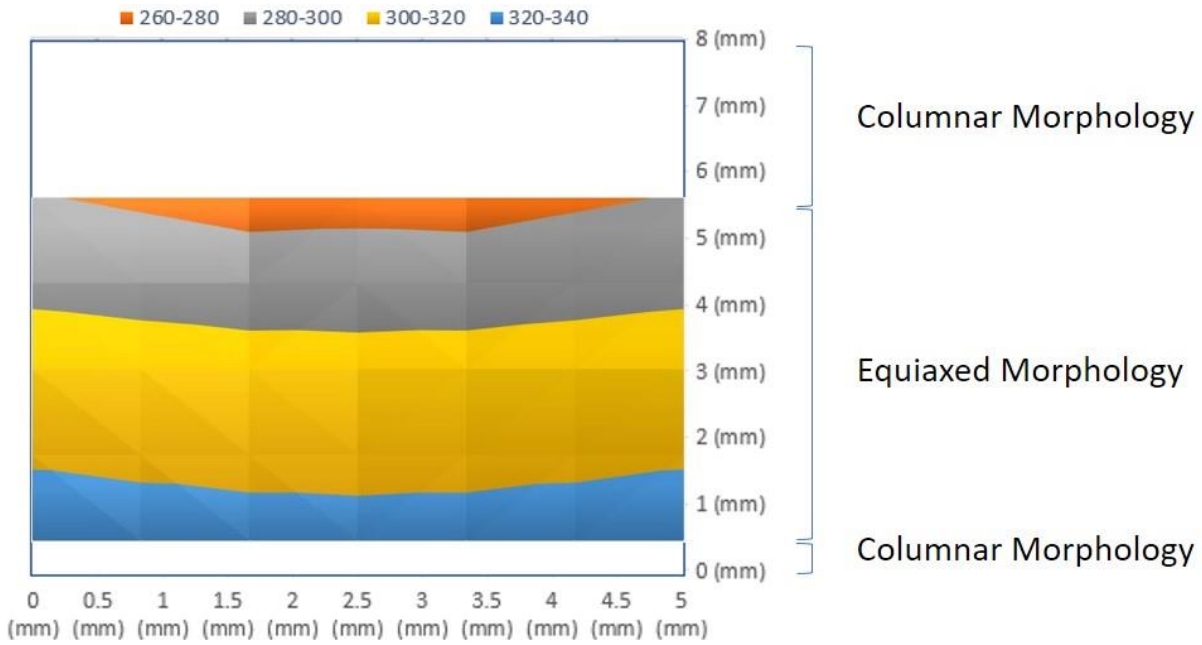

Fig. 9 – Calculated yield strength and its map at 700 C temperature of the printer's chamber.

The simulated results of grain size and yield strength at different chamber's temperatures are summarized in fig. 10. The higher chamber's temperature means larger grain size and lower yield point in the equiaxed region. Almost a fully equiaxed austenite microstructure will be achieved at 800 C

Preprints (www.preprints.org) | NOT PEER-REVIEWED | Posted: 26 August 2020 doi:10.20944/preprints202008.0573.v1

chamber's temperature, but the last printed layer, which is columnar and can be removed by cutting then. The estimated local austenite grain size and the local yield strength in the equiaxed regions are in the range of 15 to 30 µm and 270 to 330 MPa at 800 C temperature of printer's chamber, respectively.

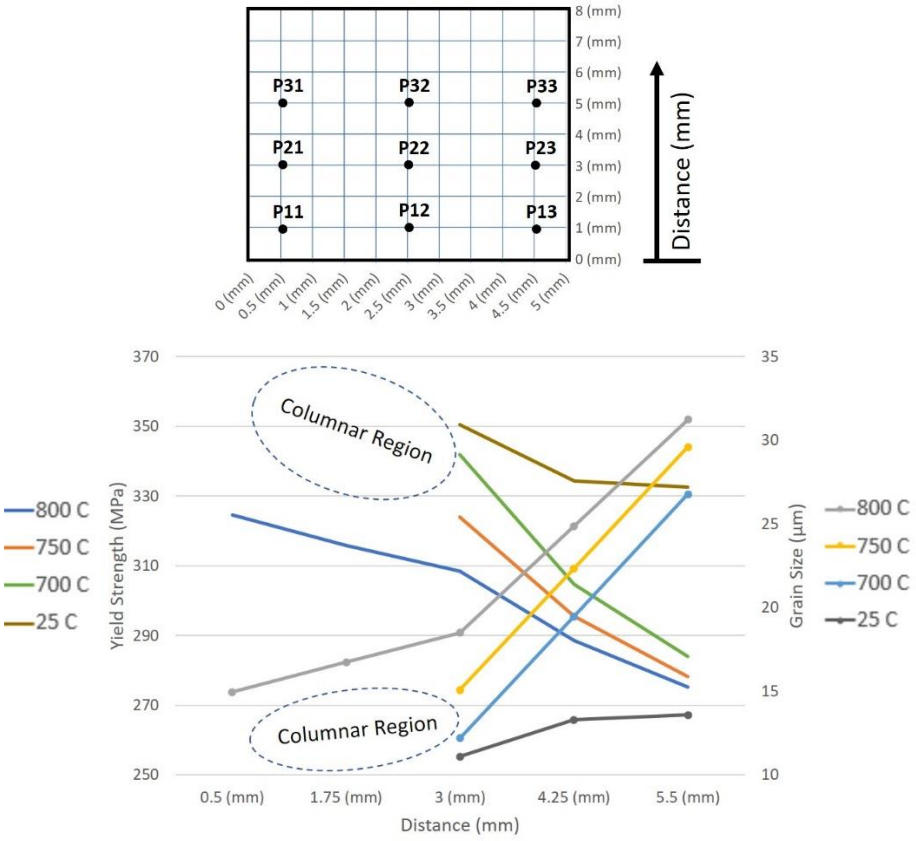

Fig. 10 – Yield strength and austenite grain size from bottom to top through the first printed layer at different temperatures of the printer's chamber.

- **Conclusions**

Metal 3D printing is an exciting manufacturing method but needs more optimizations of the printing process to have a reliable product directly for structural applications. This research tried to address the austenite grain morphology and subsequent yield strength of the printed sample. The simulation was done at constant print speed, laser power, and rate of metal powders injection but the different temperature of the printer's chamber. Simulation results show that the temperature of the printer's chamber has an effect on the microstructure of the printed sample. Highlighted computational results are as follows:

1. The austenite grain topology is more columnar at the lower temperature of the printer's chamber.
2. The percentage of the equiaxed zone will be increased at a higher chamber's temperature.
3. Almost a fully equiaxed austenite microstructure will be achieved at 800 C chamber's temperature, but the last printed layer which is columnar and can be removed by cutting then.

4. The estimated local austenite grain size and the local yield strength in the equiaxed regions are in the range of 15 to 30 µm and 270 to 330 MPa at 800 C temperature of printer's chamber, respectively.

References

1. Debroy T, Wei HL, Zuback JS, et al (2018) Progress in Materials Science Additive manufacturing of metallic components – Process , structure and properties. 92:112–224
2. Sergio M, Lima F De, Sankaré S (2014) Microstructure and mechanical behavior of laser additive manufactured AISI 316 stainless steel stringers Microstructure and mechanical behavior of laser additive manufactured AISI 316 stainless steel stringers. J Mater 55:526–532. https://doi.org/10.1016/j.matdes.2013.10.016
3. Shi X, Ma S, Liu C, et al (2017) Materials Science & Engineering A Selective laser melting-wire arc additive manufacturing hybrid fabrication of Ti-6Al-4V alloy : Microstructure and mechanical properties. Mater Sci Eng A 684:196–204. https://doi.org/10.1016/j.msea.2016.12.065
4. Pham MS, Dovgyy B, Hooper PA (2017) Materials Science & Engineering A Twinning induced plasticity in austenitic stainless steel 316L made by additive manufacturing. Mater Sci Eng A 704:102–111. https://doi.org/10.1016/j.msea.2017.07.082
5. Croteau JR, Grif S, Rossell MD, et al (2018) Acta Materialia Microstructure and mechanical properties of Al-Mg-Zr alloys processed by selective laser melting. 153:35–44. https://doi.org/10.1016/j.actamat.2018.04.053
6. Nassar AR, Reutzel EW (2015) Additive Manufacturing of Ti-6Al-4V Using a Pulsed Laser Beam. Metall Mater Trans A 46A:2781–2789. https://doi.org/10.1007/s11661-015-2838-z
7. Shamsaei N, Yadollahi A, Bian L, Thompson SM (2015) An overview of Direct Laser Deposition for additive manufacturing; Part II: Mechanical behavior, process parameter optimization and control. Addit Manuf 8:12–35. https://doi.org/10.1016/j.addma.2015.07.002
8. Li J, Cheng X, Li Z, et al (2018) Materials Science & Engineering A Improving the mechanical properties of Al-5Si-1Cu-Mg aluminum alloy produced by laser additive manufacturing with post-process heat treatments. Mater Sci Eng A 735:408–417. https://doi.org/10.1016/j.msea.2018.08.074
9. Zhuo L, Wang Z, Zhang H, et al (2019) Effect of post-process heat treatment on microstructure and properties of selective laser melted AlSi10Mg alloy. Mater Lett 234:196–200. https://doi.org/10.1016/j.matlet.2018.09.109
10. Yadollahi A, Shamsaei N, Thompson SM, Seely DW (2015) Effects of process time interval and heat treatment on the mechanical and microstructural properties of direct laser deposited 316L stainless steel. Mater Sci Eng A 644:171–183. https://doi.org/10.1016/j.msea.2015.07.056
11. Cunningham CR, Flynn JM, Shokrani A, et al (2018) Invited review article : Strategies and processes for high quality wire arc additive manufacturing. Addit Manuf 22:672–686. https://doi.org/10.1016/j.addma.2018.06.020

12. Steuben JC, Birnbaum AJ, Michopoulos JG, Iliopoulos AP (2019) Enriched analytical solutions for additive manufacturing modeling and simulation. Addit Manuf 25:437–447. https://doi.org/10.1016/j.addma.2018.10.017

13. Peng H, Ghasri-khouzani M, Gong S, et al (2018) Fast prediction of thermal distortion in metal powder bed fusion additive manufacturing : Part 1 , a thermal circuit network model. Addit Manuf 22:852–868. https://doi.org/10.1016/j.addma.2018.05.023

14. Mcmillan M, Leary M, Brandt M (2017) Computationally efficient finite difference method for metal additive manufacturing : A reduced-order DFAM tool applied to SLM. Mater Des 132:226–243. https://doi.org/10.1016/j.matdes.2017.06.058

15. Cheng L, Yang Q, Zhang P, et al (2016) Finite element modeling and validation of thermomechanical behavior of Ti- 6Al-4V in directed energy deposition additive manufacturing Finite element modeling and validation of thermomechanical behavior of Ti-6Al-4V in directed energy deposition additive . Addit Manuf 12:169–177. https://doi.org/10.1016/j.addma.2016.06.012

16. Panwisawas C, Sovani Y, Anderson MJ, et al (2016) A Multi-Scale Multi-Physics Approach to Modelling of Additive Manufacturing in Nickel-Based Superalloys. Superalloys2016 Warrendale, TMS 1021–1030. https://doi.org/10.1002/9781119075646.ch108

17. Methods C, Mech A, Yan W, et al (2018) An integrated process – structure – property modeling framework for additive manufacturing. Comput Methods Appl Mech Engrg 339:184–204. https://doi.org/10.1016/j.cma.2018.05.004

18. Zhang Z, Tan ZJ, Yao XX, et al (2018) Numerical methods for microstructural evolutions in laser additive manufacturing. https://doi.org/10.1016/j.camwa.2018.07.011

19. Michopoulos JG, Iliopoulos AP, Steuben JC, et al (2018) On the multiphysics modeling challenges for metal additive manufacturing processes. Addit Manuf 22:784–799. https://doi.org/10.1016/j.addma.2018.06.019

20. Zinovieva O, Zinoviev A, Ploshikhin V (2018) Three-dimensional modeling of the microstructure evolution during metal additive manufacturing. Comput Mater Sci 141:207–220. https://doi.org/10.1016/j.commatsci.2017.09.018

21. Rai A, Helmer H, Körner C (2017) Simulation of grain structure evolution during powder bed based additive manufacturing. Addit Manuf 13:124–134. https://doi.org/10.1016/j.addma.2016.10.007

22. Rodgers TM, Madison JD, Tikare V (2017) Simulation of metal additive manufacturing microstructures using kinetic Monte Carlo. Comput Mater Sci 135:78–89. https://doi.org/10.1016/j.commatsci.2017.03.053

23. Lu L, Sridhar N, Zhang Y (2018) Acta Materialia Phase fi eld simulation of powder bed-based additive manufacturing. Acta Mater 144:801–809. https://doi.org/10.1016/j.actamat.2017.11.033

24. Sahoo S, Chou K (2016) Phase-field simulation of microstructure evolution of Ti-6Al-4V in electron beam additive manufacturing process. Addit Manuf 9:14–24. https://doi.org/10.1016/j.addma.2015.12.005

25. Liu PW, Ji YZ, Wang Z, et al (2018) Investigation on evolution mechanisms of site-specific grain structures during metal additive manufacturing. J Mater Process Technol 257:191–202. https://doi.org/10.1016/j.jmatprotec.2018.02.042

26. Yan F, Xiong W, Faierson EJ (2017) Grain Structure Control of Additively Manufactured. 1–11. https://doi.org/10.3390/ma10111260

27. Markl M, Körner C (2016) Multiscale Modeling of Powder Bed–Based Additive Manufacturing. Annu Rev Mater Res 46:93–123. https://doi.org/10.1146/annurev-matsci-070115-032158

28. Koepf JA, Gotterbarm MR, Markl M, Körner C (2018) 3D multi-layer grain structure simulation of powder bed fusion additive manufacturing. Acta Mater 152:119–126. https://doi.org/10.1016/j.actamat.2018.04.030

29. Xia J, Jin H (2018) Advances in Engineering Software Numerical modeling of coupling thermal – metallurgical transformation phenomena of structural steel in the welding process. Adv Eng Softw 115:66–74. https://doi.org/10.1016/j.advengsoft.2017.08.011

30. Johnson KL, Rodgers TM, Underwood OD, et al (2018) Simulation and experimental comparison of the thermo-mechanical history and 3D microstructure evolution of 304L stainless steel tubes manufactured using LENS. Comput Mech 61:559–574. https://doi.org/10.1007/s00466-017-1516-y

31. Koepf JA, Gotterbarm MR, Markl M, Carolin K (2018) Acta Materialia 3D multi-layer grain structure simulation of powder bed fusion additive manufacturing. 152:. https://doi.org/10.1016/j.actamat.2018.04.030

32. Martukanitz R, Michaleris P, Palmer T, et al (2014) Toward an integrated computational system for describing the additive manufacturing process for metallic materials. Addit Manuf 1–4:52–63. https://doi.org/10.1016/j.addma.2014.09.002

33. Yan Z, Liu W, Tang Z, et al (2018) Review on thermal analysis in laser-based additive manufacturing. Opt Laser Technol 106:427–441. https://doi.org/10.1016/j.optlastec.2018.04.034

34. Haddad-Sabzevar M, Haerian A, Seied-Hossein-Zadeh H (2009) A stochastic model for austenite phase formation during arc welding of a low alloy steel. J Mater Process Technol. https://doi.org/10.1016/j.jmatprotec.2008.08.039